Finite Element Study of the Mass Transfer in Annular Reactor

Yehia M. S. El Shazly[*1], and Sarah W. Eletriby
[1]Alexandria University, Faculty of Engineering, Chemical Engineering Department, Egypt.
*yehia.elshazly@alexu.edu.eg; yehia.elshazly@hotmail.com

Abstract: The annular reactor is a very useful design to carry many chemical reactions. Its advantages such the low pressure drop and ease of temperature control renders it more desirable than traditional reactor, for example in the use as a double heat exchanger, a dialyzers or a photo-catalytic reactors, where a UV lamp can be placed in the core of the reactor. In this study, the isothermal mass transfer from the inner side of the outer tube of the annular reactor is being studied by the Finite Element technique within a range of flow rates corresponding to 200<Re<12000. The study focuses on the effect of the geometry on the rate of mass transfer in the developing flow and in the fully developed zones. The results showed that the surface mass transfer is highest at the entrance and decreases as the flow becomes fully developed. Also, the annulus diameter ratio and the inlet section dimensions were found to have an important impact on the efficiency of the reactor. These results are in agreement with previous CFD and experimental studies.

Keywords: Annular Reactor, Solid Liquid Mass Transfer, Finite Element, Developing flow, Fully developed flow.

1. Introduction

Annular reactors are being increasingly in used in chemical processes [1-4]. Its design offers many recognized advantages such as low pressure drop, large surface area to volume, easy temperature control, and nearly isothermal reaction conditions. It is important that when designing these reactors to consider the effect of the geometry on the flow pattern and its impact on mass and heat transfer occurring in the reactor. The study of the mass transfer has many practical applications: for example for the case of catalytic reactions where the rate of reaction is controlled by the diffusion of the reactants/products to or away from the surface of the catalyst. Also for the diffusion controlled corrosion where the rate of corrosion is controlled by the diffusion of the oxidizer to the surface[5]. Moreover, for the case of annular heat exchanger, the analogy between heat and mass transfer enables us to deduce heat or mass transfer from the other [6, 7].

Usually the rate of mass transfer is reported in the form of dimensional relationships relating Sherwood Number (the ratio of convective to diffusive mass transfer) with Reynolds (ratio of inertial force to viscous force) and Schmidt Numbers (the ratio of momentum diffusivity to molecular diffusivity). These correlation have been obtained experimentally by many techniques: the chemical reaction between the liquid and solid [8-10], the dissolution of the sparingly soluble solid into liquid[11-13], the electrochemical technique [14-17], adsorption [18, 19], and even have been followed with the scanning electron microscopy [20]. However, these correlations have the drawback that they are applicable only to a specific reactor configuration operated under a certain range of hydrodynamic conditions[21, 22].

CFD has also been used [23-26]: if well formulated, CFD has the advantages of being time and cost consuming, coupled to being non-intrusive and able to predict the results of tests that are not easily performed. Several mathematical models have been proposed and evaluated which included mass transfer in annular reactors used for different applications, but their systems were limited either to laminar, or to fully developed turbulent flow conditions[27-30]. However, due to the design of annular reactor, a fully developed flow is unattainable. Fortunately, developing flow is desirable as it yields favorable mass transfer conditions. On the other hand, mass transfer modelling under developing flow condition is a complex task. Esteban et al [31]studied the difference between the U and L entrance shape for the annular reactor on the rate of mass transfer using the finite volume technique and concluded that though most of the mass transfer took place near the entrance region of the reactor, but both of the two shape gave similar efficiency. They also found that among the different turbulence models, the Low Reynolds Number model gave the closest results to the experiments. In this study, the commercial CFD Comsol® was used to study the effect of the flow rate and the geometrical design (Ratio of

large diameter to small diameter, and length of entrance spacing) on the mass transfer of the internal wall of the outer tube of reactor. The study focuses on the mass transfer in the flow developing and fully developed zones. Table 1 shows the different correlations found in literature for mass transfer in the annular reactor.

2. Governing equation

In this study, the dissolution of a sparingly soluble wall (benzoic acid) was used to simulate the mass transfer from the wall. Esteban et al [31] used successfully this technique in the Finite Volume analysis with the commercial software Fluent® to determine the mass transfer in the annular reactor. The laminar flow model was used to study the flow within the range 200<***Re***<2100 and the *Low Reynolds Number turbulence* model was used for the range 2100<***Re***<12000.

It is assumed that the fluid is Newtonian fluid (water), incompressible, isothermal (298 K) and non-reactive with constant physical properties and that the reactor is operating in steady state conditions. Also, as the saturation concentration of the benzoic acid is very low, it is assumed that it does not change the physical properties of the water or the flow profile. This allowed solving the flow independently from the mass transfer: the CFD model was solved in two steps: First, the equations of continuity and motion were solved for getting the flow field across the computational domain. Then, the velocity values were kept "frozen" and the equation of conservation of species was solved using the converged flow solution. This solving strategy saves computation time and brings stability to the solution.

The equations solved by the Laminar Flow interface are the *Navier-Stokes* equations for conservation of momentum and the continuity equation for conservation of mass:

Table (1): Some correlations reported in literature for mass transfer in annuli.

Hydrodynamic Condition	**Ref.**	**Correlation**	
Laminar Flow			
Fully developed	[32]	$Sh_{av} = 1.614\,(Re.Sc.\varphi d_e/l)^{\frac{1}{3}}$	(i)
Developing	[17]	$Sh_{av} = 1.029 Re^{0.55}.Sc^{\frac{1}{3}}.(d_e/l)^{0.472}$	(ii)
	[33]	$Sh_{av} = 2.703\,(Re.Sc.\varphi d_e/l)^{\frac{1}{3}}$	(iii)
Turbulent Flow			
Fully developed	[32]	$Sh_{av} = 0.023 Re^{0.8}.Sc^{\frac{1}{3}}$	(iv)
	[34]	$Sh_{av} = 0.027 Re^{0.8}.Sc^{\frac{1}{3}}.(d_2/d_1)^{0.53}$	(v)
	[35]	$Sh_{av} = 0.145 Re^{2/3}.Sc^{\frac{1}{3}}.(d_e/l)^{0.25}$	(vi)
Developing	[17]	$Sh_{av} = 0.095 Re^{0.85}.Sc^{\frac{1}{3}}.(d_e/l)^{0.472}$	(vii)
	[33]	$Sh_{av} = 0.305 Re^{\frac{2}{3}}.Sc^{\frac{1}{3}}.(\varphi d_e/l)^{\frac{1}{3}}$	(viii)
	[34]	$Sh_{av} = 0.032 Re^{0.8}.Sc^{\frac{1}{3}}.\left[1+(d_e/l)^{\frac{2}{3}}\right](d_2/(d_1)^{0.53}$	(ix)

$$\left[\frac{\partial \rho}{\partial t}+u_j\frac{\partial \rho}{\partial x_j}\right]+\rho\frac{\partial u_j}{\partial x_j}=0$$

$$\left[\frac{\partial(\rho u_i)}{\partial t}+u_j\frac{\partial(\rho u_i)}{\partial x_j}\right]=-\frac{\partial p}{\partial x_i}+\frac{\partial \tau_{ij}}{\partial x_j}$$

where $\boldsymbol{\rho}$ is the density, $\boldsymbol{u}$ is the velocity vector, $\boldsymbol{p}$ is the pressure, and $\boldsymbol{\tau}$ is the viscous stress tensor.

For the case of the turbulent flow, the *Reynolds-averaged Navier-Stokes* equations (*RANS*) were used.

$$\frac{\partial U_j}{\partial x_j}=0$$

$$\rho\left[\frac{\partial U_i}{\partial t}+U_j\frac{\partial U_i}{\partial x_j}\right]=-\frac{\partial P}{\partial x_i}+\frac{\partial T_{ij}^{(v)}}{\partial x_j}=-\rho\left\langle u_j\frac{\partial u_i}{\partial x_j}\right\rangle$$

where $\boldsymbol{U}$ is the averaged velocity field, $\boldsymbol{P}$ is the averaged pressure, and $\boldsymbol{T}$ is the averaged viscous stress tensor.

The *Low Reynolds Number* (*LRN k-ε*) modelling approach has been chosen to solve the turbulent flow. It has an embedded wall damping effect that enables the flow modelling to be extended to the wall without the need to the wall equations used with the other turbulent flow models (i.e *k-ε*, *k-ω*) [31, 36].

For the mass transfer step, the transport of diluted species module was used. The concentration at the dissolving wall was kept constant at the saturation concentration of the benzoic acid. The mass transport equation incorporated the mass transfer due to convection using the flow profile calculated and to diffusion using the value of $\boldsymbol{D_m}$ equal to $9.3*10^{-10}$ m^2/s [37]

The conservation of species $\boldsymbol{A}$ assuming constant density and applying Reynolds method of averaging of the instantaneous fluctuating concentration is expressed as:

$$\frac{\partial \overline{C_A}}{\partial t}+\frac{\partial}{\partial x_j}\left(U_j\overline{C_A}\right)=\frac{\partial}{\partial x_j}\left(D_m\frac{\partial \overline{C_A}}{\partial x_j}\right)-\frac{\partial}{\partial x_j}\left(\overline{u_j{}'C_A{}'}\right)$$

where $\boldsymbol{C_A}$ indicates the concentration of the benzoic acid and the bar indicates a time averaged value. $\boldsymbol{u_j'}$ and $\boldsymbol{C_A'}$ are the fluctuating flow velocity and species $\boldsymbol{A}$ concentration respectively. The $\overline{u_j'C_A'}$ terms describe the turbulent mass transport, and in analogy with Fick's law. It is assumed that:

$$\left(\overline{u_j{}'C_A{}'}\right)=J_A^t=-D^t\,\nabla\overline{C_A}$$

The term $\boldsymbol{D^t}$ is called the turbulent diffusivity or eddy diffusivity. It is not a physical property of the fluid mixture like $\boldsymbol{D_m}$ but depends on the character of flow, mainly intensity of turbulence and on position in the system varying considerably from the turbulent core to the phase boundary. The quantity like momentum, energy and concentration are transported by turbulent eddies, i.e. the same mechanism, so there should be a correlation between the parameters appearing in their flux equations. Applying the Reynolds analogy between the turbulent momentum transfer and the turbulent mass transfer a dimensionless number is defined called the turbulent Schmidt number:

$$Sc^{(t)}=\frac{\mu^{(t)}}{\rho D^{(t)}}$$

In the computational fluid dynamics, many turbulence models have been developed which enable the determination of the eddy viscosity. The $Sc^{(t)}$ dimensionless number typically is close to unity [38-41] and it was decided to use the value of 0.9 in the following calculations.

3. Geometrical Model

The annular reactor geometry studied in the present work is shown in figure (1). The reactor main dimensions are: 30 mm outer tube diameter, 20 mm inner tube diameter, and 12 mm inlet diameter tube. The inlet port of the reactor was centred on the front plate and it was placed 30 mm away from the inner tube rounded front. The annular reactor had two sections on the inner wall of the outer tube that could be set at constant concentration: The first section corresponding to the reactor inlet is named section A, while the other section is named section B. This feature allowed for studying the mass transfer process at different hydrodynamic conditions along the length of the reactor. The design can be also simplified by using a 2D axisymmetric model to replace the 3 D model (figure 2).

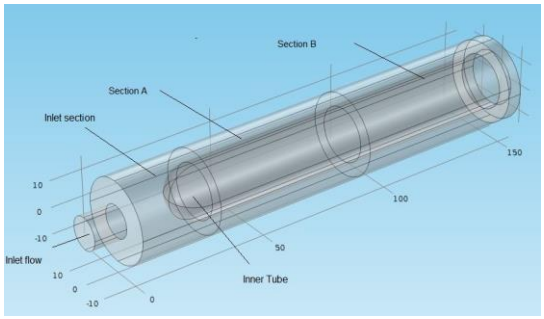

Fig. (1): Schematic diagram of the 3D annular reactor model.

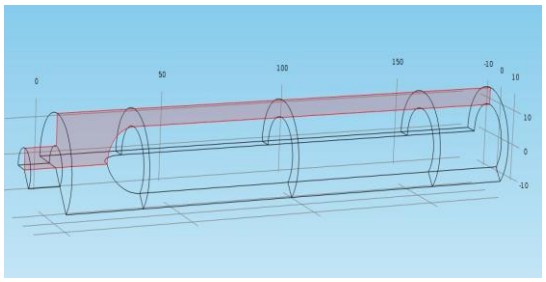

Fig. (2): Schematic diagram of the 2D axisymmetric annular reactor model, illustrating the longitudinal cut plane in the 3D model.

4. Mesh Design

For the system of the mass transfer from the wall to a turbulent fluid and for high Schmidt number, the concentration boundary layer is much smaller than the velocity boundary layer. This makes it necessary to use a very fine mesh within the near wall region using the boundary layer mesh option in Comsol. The 3D geometry is shown in Figure (3), whereas the 2D axisymmetric mesh is shown in figure (4).

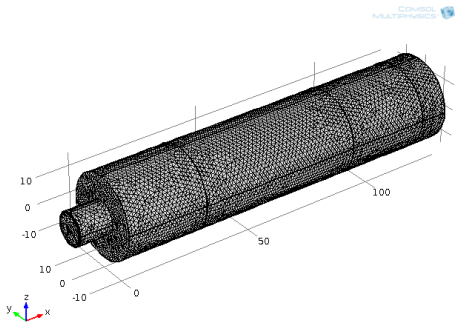

Fig. (3): Mesh utilized for the 3D geometry model.

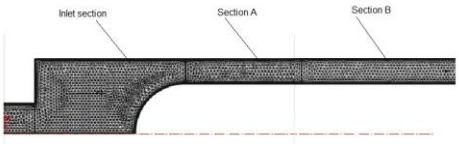

Fig. (4): Mesh utilized for the 2D axisymmetric model.

The utilized mesh was verified to give mesh – independent results: the CFD simulation results for the average mass transfer coefficient were compared with the calculated resulted from the correlation presented by Mobarak et al. [17] as shown in table (2).

Table (2): Percentage difference in the average mass transfer coefficient predicted by Mobarak et al.[17] and the CFD results for several mesh refinement for the 2D model.

Mesh	Percent Difference
Extra coarse (4317 elements)	12.97
Coarser (6742 elements)	4.43
Coarse (9331 elements)	1.89
Normal (16631 elements)	1.31
Fine (23610 elements)	1.31

5. Boundary conditions

The boundary conditions for the CFD model were defined as follows. At the inlet, the mass flow rate of the fluid was specified and the direction was defined normal to the boundary. The hydraulic diameter was fixed at 10 mm and the turbulence intensity (TI) was set with values between five and ten percent as recommended in the Comsol® CFD module user guide [41]. At all the walls, a no – slip boundary condition was imposed. Also, zero diffusive flux of species was specified at the wall, except for the walls coated with benzoic acid, where constant concentration of 27.76 mol/m^3 was fixed. This value corresponds to the saturation concentration of benzoic acid in water at 298 K [42].

The flow was either solved using the laminar flow or the low Reynolds Number turbulence models, then the velocity profile was kept frozen and the transport of diluted species was used to solve for the mass transfer from the wall.

6. Results

6.1. CFD hydrodynamic simulation:

Figure (5) shows the velocity profile along the annular reactor for (a) laminar flow corresponding to a flow rate of 1.05 Litres per minute (Re = 500), (b) turbulent flow corresponding to a flow rate of 21.04 Litres per minute (Re = 10000). It has to be mentioned that Reynolds Number was calculated based on the equivalent diameter. As seen in figure, the abrupt expansion and change of direction at the inlet zone generate large velocity gradient near the surface. The figure also shows the development of the velocity profile from the developing flow throughout the reactor inlet to the developed flow far away from the inlet effects along the annular volume.

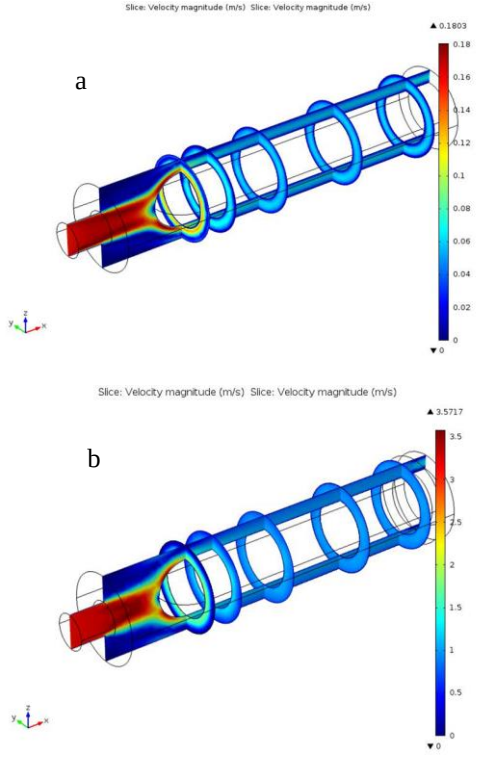

Fig. (5): Velocity magnitude (m/s) (a) laminar flow (Re = 500), (b) turbulent flow (Re = 10000).

The velocity profile was also calculated using the standard k-ε model of turbulence to compare the resultant profile with the low Reynolds model. Both of them showed similar results as seen in figure (6).

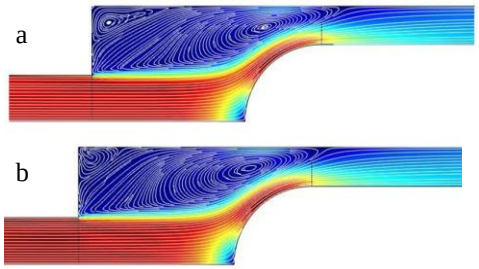

Fig. (6): Streamlines of velocity field on the longitudinal center plane at the inlet region using (a) low Reynolds k – ε turbulence model, (b) Standard k – ε turbulence model.

6.2. Average Mass Transfer

Performing a mass balance over the reactor to calculate the rate of mass transfer from the surface yields the following equation for the average mass transfer coefficient.

$$K_{av} = \frac{Q}{A} ln\left(\frac{C_{sat} - C_i}{C_{sat} - C_o}\right)$$

where Q is the flow rate, C_i and C_o are the concentrations of benzoic acid at the inlet and outlet of the reactor, respectively. The results of this work showed agreement with those from other reported investigations where similar annular configurations were used. Figure (7) and figure (8) compare the CFD predicted average mass transfer coefficients with values given by some of the correlations reported in table (1) for laminar and turbulent flows respectively.

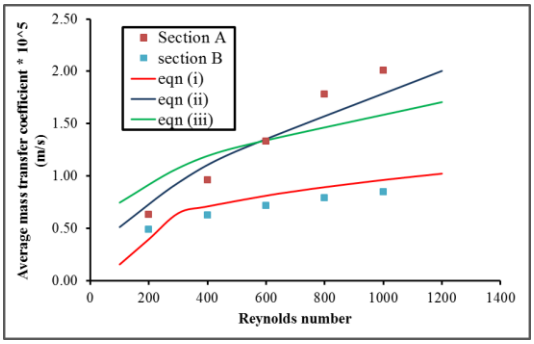

Fig. (7): Comparison of the CFD predicted average mass transfer coefficients for laminar flow with the ones estimated using different correlations reported in the literature (Table (1)).

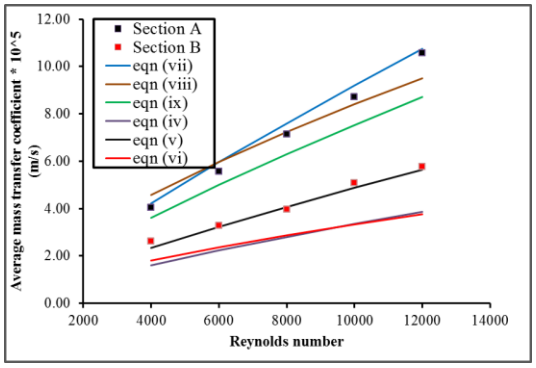

Fig. (8): Comparison of the CFD predicted average mass transfer coefficients for transitional and turbulent flows with the ones estimated using different correlations reported in the literature (Table (1)).

It is observed that the CFD predicted average mass transfer coefficients in section A were much higher than those in section B. Mass transfer coefficient in section A was nearly twice that of section B indicating the importance of the developing flow on the total mass transfer. These results suggest that the abrupt expansion and change of direction that the fluid experiences at the inlet zone generate high turbulence, as well as a large near – surface concentration gradient, which results in high mass transfer in section A. However, as the diffusion layer becomes fully developed downstream of the entrance in section B, the mass transfer decreases.

A plot of the CFD predicted value of the average mass transfer coefficient in the developing flow region for varying reactor length is given in figure (9). This figure shows the high value of the mass transfer coefficient at the leading edge (corresponding to nearly zero mass transfer boundary region) and to decrease very rapidly over the first few centimetres.
The study of the effect of the annulus diameter ratio (i.e. diameter of outer pipe to diameter of inner pipe) on the mass transfer coefficient is shown in figure (10) for section A and figure (11) for section B. The mass transfer coefficient can be seen to increase as the annulus diameter ratio decrease. This can be interpreted as when the difference between the annulus inlet and outlet diameters decreases, the surface area – to – volume ratio increase, which has a significant influence on the external mass transfer and increases the efficiency of the annular reactor.

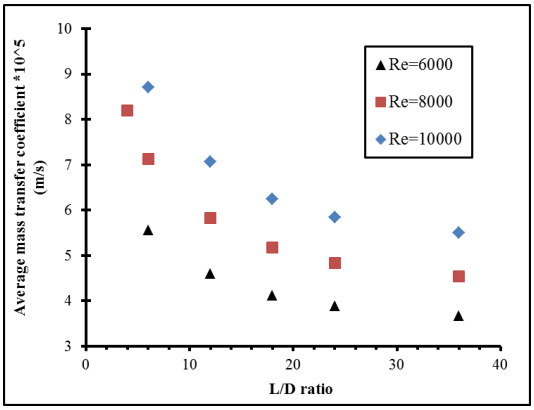

Fig. (9): Variation of the average mass transfer coefficient with the change in reactor length.

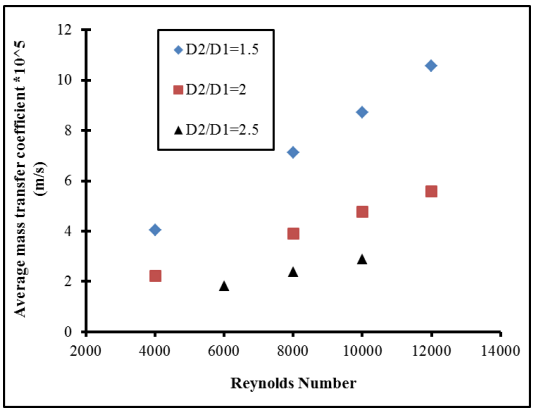

Fig. (10): Mass transfer coefficient vs. Reynolds number in section A for three different annulus diameter ratios.

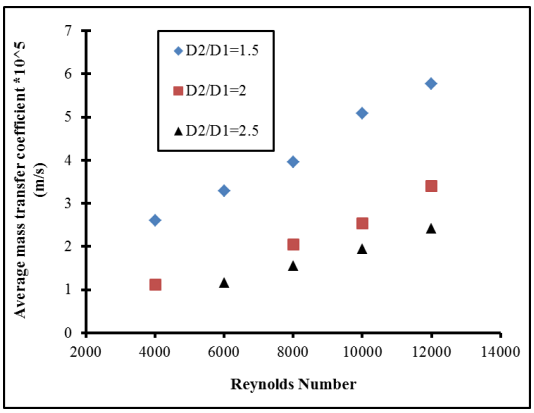

Fig. (11): Mass transfer coefficient vs. Reynolds number in section B for three different annulus diameter ratios.

The effect of the change in position of the inner tube from the inlet port on the average mass transfer coefficient in section A is shown in figure (12).

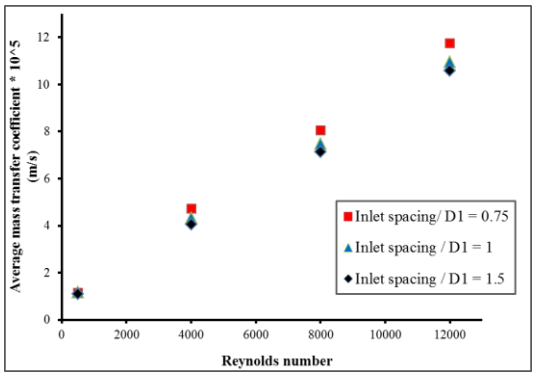

Fig. (12): Variation of the average mass transfer coefficient with the change in inlet spacing.

It is seen that as the inlet spacing decreases the mass transfer coefficient increases. This result can be interpreted by the fact that the decrease in the inlet spacing increases the intensity of abrupt expansion that the fluid experiences at the inlet zone, which in turn generates higher turbulence, as well as a larger near – surface concentration gradient, which results in a higher mass transfer in section A.

6.3. Local Mass Transfer

The local mass transfer coefficient can be estimated from the experimental correlation reported in literature by differentiating the average mass transfer coefficient by the axial distance, x [31]:

$$K_x = \frac{d\left(K_{av,x}\right)}{dx}$$

Figure 13 maps the local mass flux magnitude in section as computed utilizing the laminar flow model (*Re*=500).

Figure (14) presents the results obtained for the reactor operating at Re = 10000. As it can be seen in the figure, CFD – computed local mass transfer coefficients were consistent with those calculated from the correlations. However, for very small axial distance (x ≤ 0.005 m) some under prediction with respect to the correlations was found. This may be attributed to the weakness of the turbulence model in predicting and capturing all the small eddies generated at the inlet due to sudden expansion, separation and reattachment of the flow

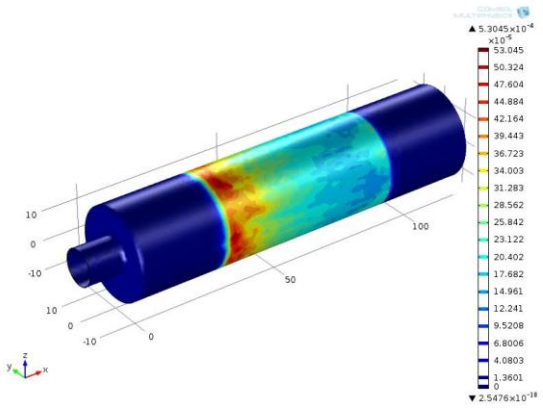

Fig (13): Local mole flux magnitude in section A for *Re*=500.

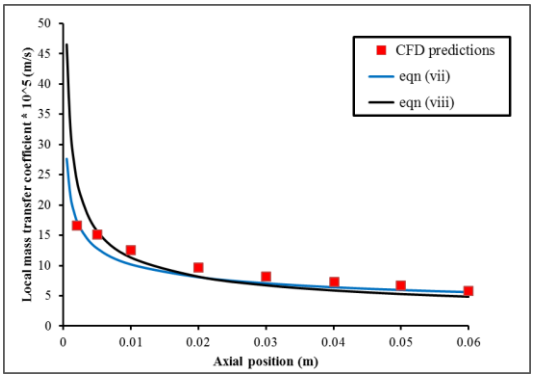

Fig. (14): CFD predictions of the local mass transfer coefficient along the reactor axis at *Re* = 10000 compared with values calculated from correlations.

7. Conclusions

In this study, CFD simulations were carried out in order to predict surface mass transfer in annular reactors within a range of flow rates corresponding to 200 < Re < 12,000 using the laminar flow model and the *Low Reynolds Number k – ε* turbulence model. The work

focused on the geometrical design factors that will affect the mass transfer in the developing flow zone and the fully developed flow zone. The CFD predicted mass transfer data obtained from this work showed good agreement with those from other reported investigations where similar annular configurations were used.

The simulations performed revealed the following results:

- The surface mass transfer taking place near the entrance region of the reactor is much higher than that happening in the rest of the reactor volume. For that reason, this section should not be ignored when considering the design of an annular reactor.
- The annulus diameter ratio was proved to have an important impact on the performance of the annular reactor. It is proved that when the difference between the annulus diameters decreases, the rate of mass transfer increases.
- As the inlet spacing between the inlet port of the reactor and the inner tube rounded front decreases, the rate of mass transfer increases.

References

1. Dalai, A.K., M.N. Esmai, and N.N. Bakhshi, *Carbon monoxide hydrogenation over cobalt catalyst in a tube-wall reactor: Part II. Modelling studies.* The Canadian Journal of Chemical Engineering, 1992. **70**(2): p. 278-285.
2. Deutschmann, O. and L.D. Schmidt, *Two-dimensional modeling of partial oxidation of methane on rhodium in a short contact time reactor.* Symposium (International) on Combustion, 1998. **27**(2): p. 2283-2291.
3. Kapteijn, F., R.M. de Deugd, and J.A. Moulijn, *Fischer–Tropsch synthesis using monolithic catalysts.* Catalysis Today, 2005. **105**(3–4): p. 350-356.
4. Houzelot J., V.J., *Mass transfer in annular cylindrical reactors in laminar flow.* Chemical Engineering Science, 1977. **32**: p. 1465 - 1470.
5. Bryan, P., *Advances in understanding hydrodynamic effects on corrosion.* Corrosion Science, 1993. **35**(1-4): p. 655-665.
6. Allan P, C., *A method of correlating forced convection heat-transfer data and a comparison with fluid friction.* International Journal of Heat and Mass Transfer, 1964. **7**(12): p. 1359-1384.
7. Yabuki, A., *Near-wall hydrodynamic effects related to flow-induced localized corrosion.* Materials and Corrosion, 2009. **60**(7): p. 501-506.
8. El Shazly, Y.M.S., *Mass transfer controlled corrosion of baffles in agitated vessels.* Corrosion Engineering, Science and Technology, 2011. **46**(6): p. 701-705.
9. Dickinson, C.F. and G.R. Heal, *Solid–liquid diffusion controlled rate equations.* Thermochimica Acta, 1999. **340-341**(0): p. 89-103.
10. Saroha, A.K., *Solid–liquid mass transfer studies in trickle bed reactors.* Chemical Engineering Research and Design, 2010. **88**(5–6): p. 744-747.
11. Askew, W.S. and R.B. Beckmann, *Heat and Mass Transfer in an Agitated Vessel.* Ind. Eng. Chem. Process Des. Dev., 1965. **4**(3): p. 311–318.
12. Shen, G.C., C.J. Geankoplis, and R.s. Brodkey, *A note on particle—liquid mass transfer in a fluidized bed of small irregular-shaped benzoic acid particles.* Chemical Engineering Science, 1985. **40**(9): p. 1797-1802.
13. Mazhar, H., et al., *Experimental investigation of mass transfer in 90° pipe bends using a dissolvable wall technique.* International Journal of Heat and Mass Transfer, 2013. **65**(0): p. 280-288.
14. Zaki, M.M., I. Nirdosh, and G.H. Sedahmed, *Mass transfer characteristics of reciprocating screen stack electrochemical reactor in relation to heavy metal removal from dilute solutions.* Chemical Engineering Journal, 2007. **126**(2-3): p. 67-77.
15. Berger, F.P. and K.F.F.L. Hau, *Mass transfer in turbulent pipe flow measured*

by the electrochemical method. International Journal of Heat and Mass Transfer, 1977. **20**(11): p. 1185-1194.
16. Sara, O.N., et al., *Electrochemical mass transfer between an impinging jet and a rotating disk in a confined system.* International Communications in Heat and Mass Transfer, 2008. **35**(3): p. 289-298.
17. Mobarak, A.A., H.A. Farag, and G. H.Sedahmed, *Mass transfer in smooth and rough annular ducts under developing flow conditions.* Journal of Applied Electrochemistry, 1997. **27**(2): p. 201-207.
18. Sonetaka, N., et al., *Characterization of adsorption uptake curves for both intraparticle diffusion and liquid film mass transfer controlling systems.* Journal of Hazardous Materials, 2009. **165**(1-3): p. 232-239.
19. Tan, C.S. and J.M. Smith, *A dynamic method for liquid-particle mass transfer in trickle beds.* AIChE Journal, 1982. **28**(2): p. 190-195.
20. Kear, G., et al., *Determination of diffusion controlled reaction rates at a solid/liquid interface using scanning electron microscopy.* Journal of Microscopy, 2007. **226**(3): p. 218-229.
21. Yunus A. Cengel, J.M.C., *Fluid Mechanics Fundamentals and Applications* 2006, New York: McGraw - Hill
22. Date, A.W., *Introduction to computational fluid dynamics*. 2005, New York: Cambridge university press.
23. Wang, J. and S.A. Shirazi, *A CFD based correlation for mass transfer coefficient in elbows.* International Journal of Heat and Mass Transfer, 2001. **44**(9): p. 1817-1822.
24. Davis, C. and P. Frawley, *Modelling of erosion–corrosion in practical geometries.* Corrosion Science, 2009. **51**(4): p. 769-775.
25. Khosravi Nikou, M.R. and M.R. Ehsani, *Turbulence models application on CFD simulation of hydrodynamics, heat and mass transfer in a structured packing.* International Communications in Heat and Mass Transfer, 2008. **35**(9): p. 1211-1219.
26. Moraveji, M.K., et al., *Experimental investigation and CFD simulation of turbulence effect on hydrodynamic and mass transfer in a packed bed airlift internal loop reactor.* International Communications in Heat and Mass Transfer, 2011. **38**(4): p. 518-524.
27. Ould-Rouis, M., et al., *Etude numérique et expérimentale des transferts de matière et de quantité de mouvement dans un écoulement annulaire laminaire non établi.* International Journal of heat and mass transfer, 1995. **38**(6): p. 953-967.
28. Farias, S.R., Legentilhomme, P., & Legrand, J. , *Finite element simulation of mass transfer in laminar swirling decaying flow induced by means of a tangential inlet in an annulus.* Computer Methods in Applied Mechanics and Engineering, 2001. **190**: p. 4713 - 4731.
29. Imoberdorf, G., Cassano, A., Irazoqui, H., & Alfano, O. , *Optimal design and modeling of annular photocatalytic wall reactors.* Catalysis Today, 2007. **129**: p. 118–126.
30. Legrand, J., & Martemyanov, S. A., *mass transfer in small radius ratio annuli.* Journal of Applied Electrochemistry, 1994. **24**(8): p. 737–744.
31. Esteban Duran, J., F. Taghipour, and M. Mohseni, *CFD modeling of mass transfer in annular reactors.* International Journal of Heat and Mass Transfer, 2009. **52**(23-24): p. 5390-5401.
32. Ross, T.K. and A.A. Wragg, *Electrochemical mass transfer studies in annuli.* Electrochimica Acta, 1965. **10**(11): p. 1093-1106.
33. Ghosh, U. and S. Upadhyay, *Mass Transfer to Newtonian and Non-Newtonian Fluids in Short Annuli.* AIChE Journal, 1985. **31**(10): p. 1721 - 1724.
34. Rai, B.N., et al., *Forced convective mass transfer in annuli.* Chemical Engineering Communications, 1988. **68**(1): p. 15-30.
35. Pickett, D.J., *Electrochemical reactor design / David J. Pickett*. Chemical

engineering monographs ; v. 9. 1979: Elsevier Pub. Co. .
36. Frei, W. *http://www.comsol.com/blogs/which-turbulence-model-should-choose-cfd-application/*. 2013 [cited 2014 24/05].
37. Noulty, R.A. and D.G. Leaist, *Diffusion coefficient of aqueous benzoic acid at 25.degree.C.* Journal of Chemical & Engineering Data, 1987. **32**(4): p. 418-420.
38. Launder, B.E., *Heat and mass transport*, in *Turbulence*, P. Bradshaw, Editor. 1978, Springer Berlin Heidelberg. p. 231-287.
39. Koeltzsch, K., *The height dependence of the turbulent Schmidt number within the boundary layer.* Atmospheric Environment, 2000. **34**(7): p. 1147-1151.
40. Reynolds, A.J., *The prediction of turbulent Prandtl and Schmidt numbers.* International Journal of heat and mass transfer, 1975. **18**(9): p. 1055-1069.
41. Comsol, *Comsol 4.3 CFD Module User's guide*. 2012.
42. Yalkowsky, S.H., *Handbook of Aqueous Solubility Data*. 2003: Taylor & Francis.